JOURNAL OF SYNCHROTRON RADIATION
ISSN 1600-5775

Fluorescence imaging of reactive oxygen species by confocal laser scanning microscopy for track analysis of synchrotron X-ray photoelectric nanoradiator dose: X-ray pump–optical probe

Jae-Kun Jeon,[a] Sung-Mi Han[b] and Jong-Ki Kim[a]*

[a]Department of Biomedical Engineering, School of Medicine, Catholic University of Daegu, Daegu 42472, Republic of Korea, and [b]Department of Anatomy, School of Medicine, Catholic University of Daegu, Daegu 42472, Republic of Korea. *Correspondence e-mail: jkkim@cu.ac.kr

Received 17 May 2016
Accepted 6 June 2016

Edited by S. M. Heald, Argonne National Laboratory, USA

Keywords: X-ray photoelectric; nanoradiator effect; ROS fluorescence; gel dosimetry; confocal laser scanning.

Bursts of emissions of low-energy electrons, including interatomic Coulomb decay electrons and Auger electrons (0–1000 eV), as well as X-ray fluorescence produced by irradiation of large-Z element nanoparticles by either X-ray photons or high-energy ion beams, is referred to as the nanoradiator effect. In therapeutic applications, this effect can damage pathological tissues that selectively take up the nanoparticles. Herein, a new nanoradiator dosimetry method is presented that uses probes for reactive oxygen species (ROS) incorporated into three-dimensional gels, on which macrophages containing iron oxide nanoparticles (IONs) are attached. This method, together with site-specific irradiation of the intracellular nanoparticles from a microbeam of polychromatic synchrotron X-rays (5–14 keV), measures the range and distribution of OH radicals produced by X-ray emission or superoxide anions (O_2^-) produced by low-energy electrons. The measurements are based on confocal laser scanning of the fluorescence of the hydroxyl radical probe 2-[6-(4′-amino)phenoxy-3*H*-xanthen-3-on-9-yl] benzoic acid (APF) or the superoxide probe hydroethidine-dihydroethidium (DHE) that was oxidized by each ROS, enabling tracking of the radiation dose emitted by the nanoradiator. In the range 70 µm below the irradiated cell, $^{\bullet}$OH radicals derived mostly from either incident X-ray or X-ray fluorescence of ION nanoradiators are distributed along the line of depth direction in ROS gel. In contrast, O_2^- derived from secondary electron or low-energy electron emission by ION nanoradiators are scattered over the ROS gel. ROS fluorescence due to the ION nanoradiators was observed continuously to a depth of 1.5 mm for both oxidized APF and oxidized DHE with relatively large intensity compared with the fluorescence caused by the ROS produced solely by incident primary X-rays, which was limited to a depth of 600 µm, suggesting dose enhancement as well as more penetration by nanoradiators. In conclusion, the combined use of a synchrotron X-ray microbeam-irradiated three-dimensional ROS gel and confocal laser scanning fluorescence microscopy provides a simple dosimetry method for track analysis of X-ray photoelectric nanoradiator radiation, suggesting extensive cellular damage with dose-enhancement beyond a single cell containing IONs.

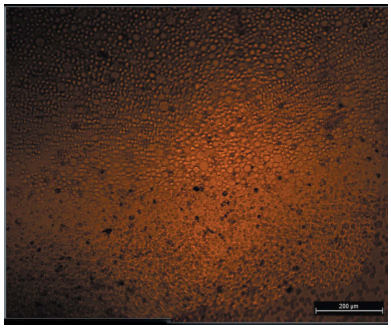

1. Introduction

Irradiation of nanoparticles composed of large-Z elements with X-ray photons or high-energy charged particles ionizes the atoms in the nanoparticles. Following ionization, bursts of low-energy electrons and X-ray photons are emitted through an Auger cascade process involving atoms that have been directly ionized and through interatomic de-excitation of adjacent neutral atoms that have been ionized (Kim *et al.*, 2012; Gokhberg *et al.*, 2014; Seo *et al.*, 2015). This process

provides the means to increase the effect of single atomic ionization. When this emission, termed the nanoradiator effect, occurs in a target tissue or in a radiation-receiving device, the high production of electrons can greatly increase the therapeutic efficiency of radiation therapy *via* dose enhancement. It is therefore necessary to quantify the dose enhancement and to investigate the dose distribution in order to establish a therapeutic treatment employing nanoradiators. In a previous report (Seo *et al.*, 2015), the physical mechanism underlying the dose enhancement was elucidated by using a fluorescent probe for reactive oxygen species (ROS). We found that the mechanism increased the ROS production in aqueous solution of a van der Waals contact atomic cluster due to interatomic Coulomb decay. When the fluorescent probes are immobilized inside a gel, fluorescence measurement of the ROS produced by the nanoradiator may enable discrete track analysis along the radiation path as energy transfers from the emitted radiation to the ROS. This method is in contrast to simply quantifying the overall dose induced by the nanoradiator in an aqueous solution. It is also desirable to analyze the process of energy transfer occurring in a single cell, from the absorption of incident X-rays by large-Z nanoparticles to the nanoradiator effect that follows, in order to understand how nanoradiator-mediated radiation propagates into the surrounding medium. In this work, individual cells containing iron oxide nanoparticles (IONs) were grown on the surface of three-dimensional (3D) ROS gels containing fluorescent probes. IONs, which act as the photoelectric nanoradiator, were activated by a microbeam of polychromatic synchrotron X-rays. Energy transfer from the incident X-rays mediated by the nanoradiator, manifested as the fluorescence of the ROS, was analyzed by confocal laser scanning microscopy along the depth of propagation of radiation as track analysis.

2. Methods and materials

2.1. 3D ROS gels

Gels containing the fluorescent probes, here termed ROS gels, were prepared by using agarose gel in a 1 ml tub, which was embedded in rubber clay, as shown in Fig. 1. Prior to gel formation, agarose solutions (0.2%) containing either 5 µ*M* 2-[6-(4′-amino)phenoxy-3*H*-xanthen-3-on-9-yl] benzoic acid (APF) or 100 µ*M* hydroethidine-dihydroethidium (DHE) solution were magnetically stirred at 40°C in a nitrogen environment for mixing homogeneously. Macrophages were incubated with a 1 mg ml^{-1} solution of IONs for 24 h in a Petri dish and then washed several times with the culture medium. The cells containing IONs were harvested and seeded again with the culture medium onto the surface of the agarose gel coated with poly L-lysine, and incubated for 24 h. After cell growth was confirmed by fluorescence microscopy as illustrated in Fig. 2, the gel (APF-ION gel, DHE-ION gel) was mounted on the sample holder. Similar gel phantoms (*i.e.* without ION uptake; APF gel, DHE gel) were prepared for control experiments.

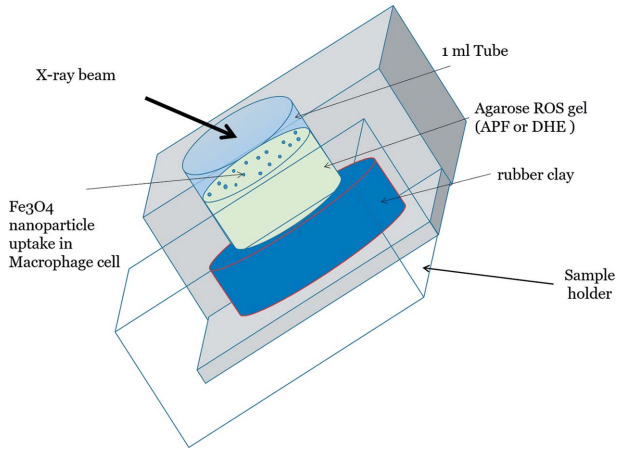

Figure 1
Schematic diagram of the construction of the 3D ROS gel. The gel was contained in a 1 ml tube that was embedded in rubber clay for attachment to the sample holder.

2.2. Scanning transmission X-ray microscopy (STXM)

Macrophage uptake and the intracellular distribution of IONs were investigated separately *in vacuo* by using the synchrotron-radiation-based STXM technique on the cell grown in a silicon nitride window at the PAL 10A bending-magnet beamline (Pohang, Korea). Either cell or ION was imaged based on the absorption of scanning zone-plate nano-focused soft X-rays of energy 542 eV near the C-K line or 714 eV near the Fe-L line X-rays, respectively.

2.3. Intracellular nanoparticle concentration of iron oxide nanoparticles

The cellular uptake of iron oxide nanoparticles was measured as a function of the incubating concentration (0, 0.2,

Figure 2
Fluorescence microscopy image of macrophages containing Fe_3O_4 nanoparticles grown on the surface of agarose gel coated with poly L-lysine. A cell was selected for irradiation with an X-ray microbeam at a marked distance from the edge of the sample holder window.

Table 1
Intracellular concentration of Fe_3O_4 nanoparticles (IONs).

The average number of IONs per cell was calculated based on an ION size of 13 nm with an average of 6000 Fe atoms per single ION. The average weight per ION was calculated to be 3.48×10^{-19} g.

Cell number ($\times 10^6$)	ION incubation (μg ml^{-1})	Fe uptake density (μg per 10^6 cells)	ION number ($\times 10^7$ per cell)
3.9	20	0.64	0.18
3.9	200	2.31	0.66
3.6	500	3.88	1.11
3.0	1000	6.53	1.87
2.5	2000	15.38	4.42

0.5, 1.0 and 2.0 mg ml^{-1}) using an inductively coupled plasma (ICP-MS) mass spectrometer (Thermo Jarrell Ash ARISAP, USA). A total of 2.5×10^6 to 3.9×10^6 macrophage cells were plated in separate Petri dishes containing different concentrations of the nanoparticle solution. The measured data were presented as the average uptake density (μg Fe per 10^6 cells) in each incubating dose after harvesting the cells for the ICP-MS measurements.

2.4. Photoelectric nanoradiator

X-ray irradiation of a selected cell containing IONs was carried out *in vacuo* using synchrotron radiation at the PAL 4B bending-magnet beamline. The entire area of the selected cell was probed using a scanning polychromatic (5–14 keV) microbeam with a diameter of 5 μm. Since the typical size of the macrophage cell was estimated to be 10 μm, the X-ray beam scanned four times to cover the entire area of the cell. The radiation dose was measured with a UNIDOSE dosimeter using a Farmer-type chamber, and the total exposure was carried out for 3 s at a dose rate of 240 mGy s^{-1}. A cell selected in each ROS gel phantom (APF-ION gel, APF gel, DHE-ION gel, DHE gel) was irradiated at the same position in the sample holder to ensure an identical environment of primary incidence X-rays.

2.5. Confocal laser scanning microscopy

Irradiated agarose ROS gel was sectioned to samples of thickness 200 μm using a microtome (Micro Slicer, DTK-2000, DSK). Sectioned samples were mounted on microscopy slides, and fluorescence by either APF (λ_{em} = 532 nm) or DHE (λ_{em} = 635 nm) was examined under a confocal laser scanning fluorescence microscope (Nikon, A1). The fluorescence intensity was analyzed using the default software of the confocal microscope, and its track was plotted using *Amira* software (VSG Inc., Burlington, USA) for image processing.

3. Results and discussion

IONs were taken up in the macrophage cell in an incubation-dose-dependent manner (Table 1), and distributed in the cell as shown by the X-ray absorption contrast of the STXM image in Fig. 3. Since typical IONs have a diameter of 13 nm, they did not enter the nucleus, as shown in Fig. 3(*b*). The intracellular distribution of Fe_3O_4 nanoparticles was inhomogeneous, and different for each cell. Therefore, the obtained ROS fluorescence imaging of the gel represented the nanoradiator track from a typical intracellular distribution of IONs in a selected cell for irradiation with X-ray microbeam.

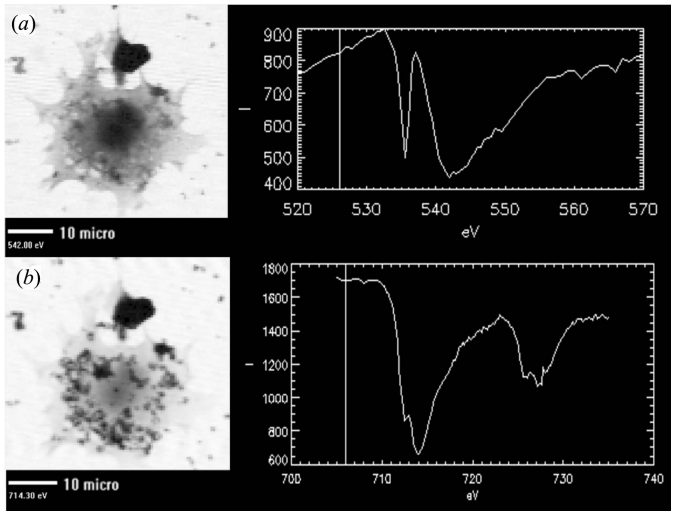

Figure 3
STXM absorption-based imaging of a macrophage cell at 542 eV near the C 1*K*-line X-ray energy (*a*) and intracellular distribution of Fe_3O_4 nanoparticles with 714 eV near the Fe *L*-edge X-ray energy (*b*).

As shown in Fig. 4, the ROS distribution was characterized on the basis of fluorescence of APF at λ_{em} = 532 nm and DHE at λ_{em} = 635 nm after their oxidation by the hydroxyl radical and superoxide, respectively, which, in turn, were generated either by primary incident X-rays alone or by X-rays and electrons emitted by the combined nanoradiator, respectively. Fluorescence from the ROS gel containing IONs showed relatively more areas of intensity compared with those of the ROS gel without IONs, as shown in Fig. 4. This trend became pronounced in the plot of relatively longer range as demonstrated in Fig. 6. This difference suggests that the nanoradiator effect involving IONs enhanced the production of the hydroxyl radicals or superoxide during the passage of propagation. These results are consistent with the dose enhancement by large-*Z* nanoparticles irradiated with X-rays, as shown in previous reports (Choi *et al.*, 2012; Carter *et al.*, 2007; Hainfeld *et al.*, 2008; Leung *et al.*, 2011; Lechtman *et al.*, 2011). In addition, $^{\bullet}$OH radicals derived mostly from either incident X-rays or X-ray fluorescence of ION nanoradiators are distributed along the line of depth direction in the ROS gel as evident from plotting the APF fluorescence in Figs. 5(*a*) and 5(*b*). In contrast, O_2^- derived from secondary electron or low-energy electron emission by ION nanoradiators are scattered over the ROS gel. Multiple areas of ROS-based fluorescence were converted into single-spot fluorescence at the depth of 50–70 μm below the gel surface as shown in Fig. 5(*c*). Three ROS tracks, except the $^{\bullet}$OH track from incident X-rays, showed a similar angular direction. This suggested the generation of either O_2^- or $^{\bullet}$OH commonly from X-ray

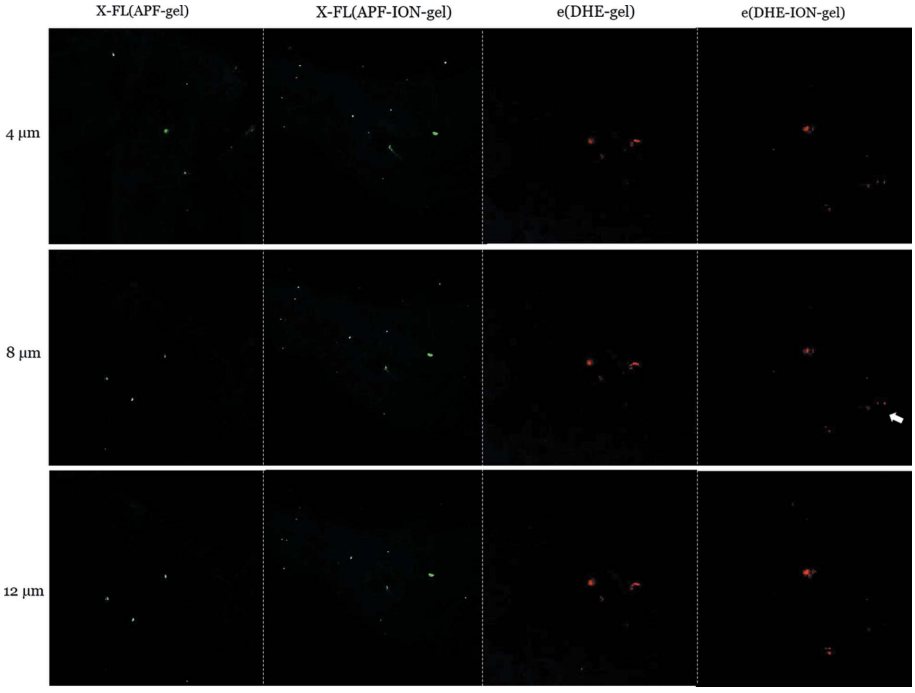

Figure 4
Planar ROS distribution from either X-ray or electron emission in a short range of depth from the site of generation inside a cell, detected by APF gel or DHE gel under X-ray irradiation in either the absence or presence of IONs. This demonstrates multiple scattered $^{\bullet}OH$ or O_2^- in the planes at some gel depths under X-ray irradiation in the presence of intracellular IONs.

fluorescence of ION nanoradiators since nanoradiator-mediated low-energy electrons (<10 keV) could not migrate by more than 100 μm. Therefore, DHE fluorescence due to O_2^- beyond 100 μm could be attributed to the production of secondary electrons from the X-ray fluorescence of ION nanoradiators. Interestingly, the area of the APF or DHE fluorescence measured in the sectioned gel increased with the depth of the radiation track, but decreased in overall intensity, indicating diffuse scattering of the X-ray photons emitted by the nanoradiator as they propagate through the gel (Fig. 6). APF fluorescence had a relatively higher intensity with larger area compared with DHE fluorescence at depths beyond 100 μm. This indicated partial production of secondary electrons from X-ray fluorescence of ION nanoradiators which in turn generated O_2^- that was detected by DHE fluorescence. The relative intensity of APF fluorescence just beneath the irradiated cell was slightly weak compared with DHE fluorescence, indicating that the X-ray photoelectric nanoradiator, IONs, emits fewer electrons than X-ray fluorescence; the higher fluorescence intensity of the ROS probe is correlated with an enhanced production of radicals generated by X-rays or electrons emitted by the nanoradiator. The composition of the emitted radiation from the nanoradiator may be dependent on the *Z*-number of its atoms. As reported by Misawa & Takahashi (2011), nanoradiator gold nanoparticles produced 5.6 times more superoxide compared with hydroxyl radicals from emitted electrons and X-rays. This difference in emission composition between the nanoradiators gold and IONs is presumably due to the much higher *Z*-number of gold, which effectively leads to more electrons emitted from Auger cascades and intermolecular/interatomic Coulombic decay (Gokhberg *et al.*, 2014; Seo *et al.*, 2015), as has been demonstrated theoretically (Pradhan *et al.*, 2009).

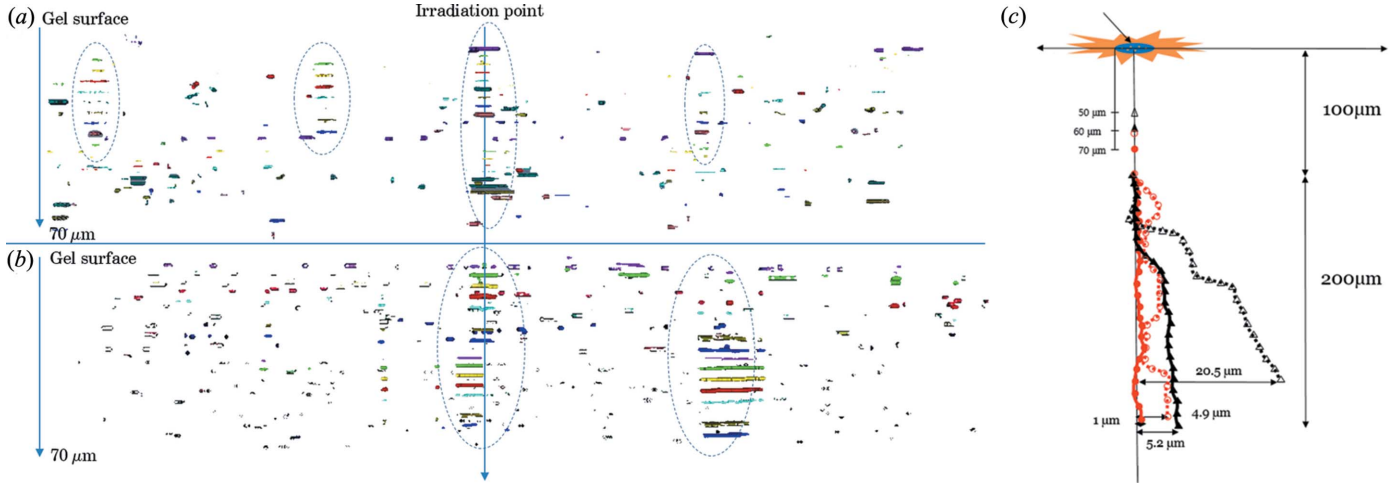

Figure 5
ROS distribution from either X-ray or electron emission in the depth direction of the ROS gel from the site of generation inside a cell, detected by APF gel or DHE gel under X-ray irradiation in either the absence (*a*) or presence (*b*) of IONs. A large ROS production appeared within a certain distance from the site of impact just beneath the cell; then it penetrated further in a different angular direction as a single track of either superoxide or hydroxyl radicals (*c*).

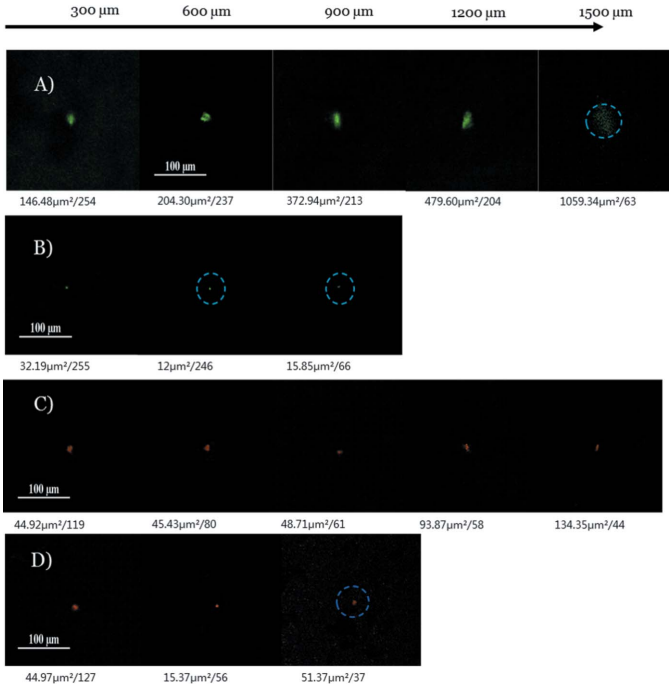

Figure 6
Images of ROS fluorescence in each 3D ROS gel section for the hydroxyl radical (*a*) and superoxide (*c*) produced, respectively, by X-rays and low-energy electrons emitted by the nanoradiators, IONs, inside a single X-ray-irradiated macrophage. Fluorescence images of (*c*) hydroxyl radicals and (*d*) superoxide produced by incident primary X-rays in an aqueous environment.

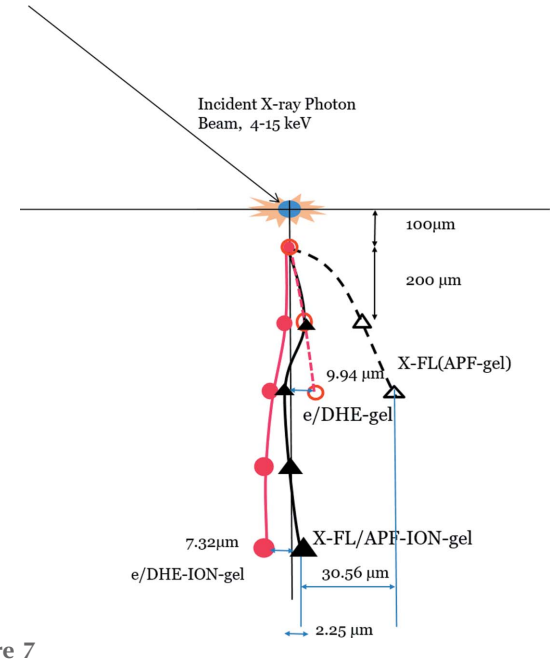

Figure 7
Tracks of the radiation emitted by the nanoradiator along the depth of the ROS gel showing different depths and angular directions of penetration of X-rays and low-energy electrons in the ROS fluorescent gel; X-rays–$^{\bullet}$OH was detected by APF green fluorescence and low-energy electrons–O_2^- was detected by DHE red fluorescence. ROS derived from the ION nanoradiator in a single cell extended beyond the dimensions of a single cell, suggesting more biological damage in the surrounding medium.

The track of the radiation emitted by the nanoradiator could be determined by plotting the fluorescence intensity in each gel slice along the depth of the ROS gel (see Figs. 5 and 7). Fluorescence resulting from ROS production by the nanoradiators was observed continuously to a depth of 1.5 mm for both APF-ION gel and DHE-ION gel, whereas the fluorescence from the ROS produced solely by incident X-rays (*i.e.* without ION) was limited to a depth of 600 µm. Most of the incident X-ray photons with energy 5–14 keV were attenuated rapidly by the water on the surface and the bulk of the gel, while producing hydroxyl radicals and superoxide from interaction of X-ray photons with water molecules. In addition, ROS generated in the aqueous phase may migrate to the surface of the ROS gel. Attachment of the macrophages with IONs to the gel surface resulted in a longer track of X-rays or electrons emitted by the nanoradiators. ION nanoradiators provided a new radiation source like an internal emitter from the gel surface, and led to deeper penetration and different angular distribution of the radiation inside the gel compared with irradiation from the primary incident X-ray beam. In general, the radiation emitted by the nanoradiators propagated in a direction different from that of the incident X-ray beam used to irradiate the sample at a fixed incident angle. Electrons emitted by the nanoradiator effect had mostly low energy (less than several hundreds of electronvolts), resulting in a relatively short penetration depth (typically less than 100 µm) from the site of generation. Hence, the track of the fluorescence from DHE reaching a depth of 1.5 mm may suggest a mix of processes producing the superoxide. In addition to superoxide produced by electrons directly emitted by the nanoradiator, superoxide could also be derived from either secondary electrons or hydroxyl radicals, which had been formed by X-ray fluorescence emitted by the nanoradiator at the depth where the ROS fluorescence was detected. This result suggests that tissue damage caused by nanoradiators in cells can extend beyond the dimensions of a single cell.

4. Conclusions

A method that combines the use of 3D ROS gel and confocal laser scanning fluorescence microscopy provides a new dosimetry-based track analysis of the radiation emitted by a nanoradiator. This method was demonstrated here by using ION-containing single cells that had been irradiated with an X-ray microbeam and analyzed by micrometer-scale laser scanning. Compositional and depth profile analyses of the radiation may determine the extent of cellular damage with respect to the different large-Z nanoparticles. The ROS fluorescence due to ION nanoradiators showed a dose-enhancement effect as well as a higher penetration by nanoradiators, which may lead to extended cellular damage.

Acknowledgements

This work was performed with financial support from the National Research Foundation of Korea funded by

the Ministry of Education, Science and Technology (2013M2B2B1075774 and 2015M2A2A7A1045270).

References

Carter, J. D., Cheng, N. N., Qu, Y., Suarez, G. D. & Guo, T. (2007). *J. Phys. Chem. B*, **111**, 11622–11625.
Choi, G.-H., Seo, S.-J., Kim, K.-H., Kim, H.-T., Park, S.-H., Lim, J.-H. & Kim, J.-K. (2012). *Radiat. Oncol.* **7**, 184–194.
Hainfeld, J. F., Dilmanian, F. A., Slatkin, D. N. & Smilowitz, H. M. (2008). *J. Pharm. Pharmacol.* **60**, 977–985.
Kim, J.-K., Seo, S.-J., Kim, H.-T., Kim, K.-H., Chung, M.-H., Kim, K.-R. & Ye, S.-J. (2012). *Phys. Med. Biol.* **57**, 8309–8323.
Gokhberg, K., KolorenCU, P. E., Kuleff, A. I. & Cederbaum, L. S. (2014). *Nature (London)*, **505**, 661–663.
Lechtman, E., Chattopadhyay, N., Cai, Z., Mashouf, S., Reilly, R. & Pignol, J. P. (2011). *Phys. Med. Biol.* **56**, 4631–4647.
Leung, M. K. K., Chow, J. C. L., Chithrani, B. D., Lee, M. J. G., Oms, B. & Jaffray, D. A. (2011). *Med. Phys.* **38**, 624–631.
Misawa, M. & Takahashi, J. (2011). *Nanomed. Nanotechnol. Biol. Med.* **7**, 604–614.
Pradhan, A. K., Nahar, S. N., Montenegro, M., Yu, Y., Zhang, H. L., Sur, C., Mrozik, M. & Pitzer, R. M. (2009). *J. Phys. Chem. A*, **113**, 12356–12363.
Seo, S.-J., Han, S.-M., Cho, J.-H., Hyodo, K., Zaboronok, A., You, H., Peach, K., Hill, M. A. & Kim, J.-K. (2015). *Radiat. Environ. Biophys.* **54**, 423–431.